Virtual-State Model for Analyzing Electro-Optical Modulation in Ring Resonators

Zhengyi Wan,[1,*] Qizhuang Cen,[2,3,4,*] Yuedi Ding,[5] Shiqi Tao,[5] Cheng Zeng,[5] Jinsong Xia,[5] Kun Xu,[1] Yitang Dai,[1,†] and Ming Li[2,3,4,‡]

[1]*State Key Laboratory of Information Photonics and Optical Communications, Beijing University of Posts and Telecommunications, Beijing 100876, China*

[2]*Key Laboratory of Optoelectronic Materials and Devices, Chinese Academy of Sciences, Beijing 100083, China*

[3]*School of Electronic, Electrical and Communication Engineering, University of Chinese Academy of Sciences, Beijing 100049, China*

[4]*Center of Materials Science and Optoelectronics Engineering, University of Chinese Academy of Sciences, Beijing 100190, China*

[5]*Wuhan National Laboratory for Optoelectronics, Huazhong University of Science and Technology, Wuhan 430074, China*

(Received 12 June 2023; accepted 21 February 2024; published 22 March 2024)

Ring resonators play a crucial role in optical communication and quantum technology applications. However, these devices lack a simple and intuitive theoretical model to describe their electro-optical modulation. When the resonance frequency is rapidly modulated, the filtering and modulation within a ring resonator become physically intertwined, making it difficult to analyze the complex physical processes involved. We address this by proposing an analytical solution for electro-optic ring modulators based on the concept of a "virtual state." This approach equates a lightwave passing through a dynamic ring modulator to one excited to a virtual state by a cumulative phase and then returning to the real state after exiting the static ring. Our model simplifies the independent analysis of the intertwined physical processes, enhancing its versatility in analyzing various incident signals and modulation formats. Experimental results, including resonant and detuning modulation, align with the numerical simulation of our model. Notably, our findings indicate that the dynamic modulation of the ring resonator under detuning driving approximates phase modulation.

DOI: 10.1103/PhysRevLett.132.123802

Introduction.—Electro-optic (EO) modulation, which rapidly modulates optical signals using electrical signals, is a critical technique in optical applications including optical interconnects [1,2], optical computing [3], microwave photonics [4], and laser detection and ranging [5,6]. Standard traveling-wave EO modulators rely on length-dependent modulation accumulation due to unidirectional lightwave propagation in waveguides, which poses challenges for large-scale on-chip integration. However, recent optoelectronic integration advancements have drawn attention to the EO modulation of optical resonators. The resonance effect allows for the utilization of optical feedback to enhance modulation efficiency. On-chip resonators featuring ultra-high-quality factors (Q factors) and compact mode volumes have gained broad application in nonlinear optics [7,8], cavity quantum electrodynamics [9,10], and optomechanics [11]. This high-efficiency modulation has facilitated the development of high-performance EO modulators with a tuning efficiency of 1.98 GHz/V and a bandwidth of 17.5 GHz [12]. A recent demonstration showcased the use of an ultra-low-loss thin-film lithium niobate resonator to create an optical frequency comb (OFC) with over 900 lines [13]. EO modulation in coupled resonators has revealed a range of intriguing physical phenomena, including Rabi oscillations, Ramsey interference, Autler-Townes splitting, and Stark shifts [14], leading to the development of innovative devices such as photonic two-level systems [14] and frequency beam splitters [15].

Unraveling the physical interaction between lightwaves and electricity, EO modulation necessitates a simple and universally applicable theoretical model. A clear, intuitive model simplifies computations and provides a concise description of complex physical processes. For instance, in traveling-wave modulation, the output lightwave can be calculated by directly multiplying the input lightwave with the electrical signal, and adjusting the amplitude, phase, frequency, or polarization of the lightwave accordingly. However, dynamic EO modulation of the ring lacks a straightforward model due to the need to account for multiple-phase modulation and interference from lightwave cycling within the ring. If the lifetime of cavity photons is considerably shorter than the modulation period, the ring can be utilized as an amplitude modulator. This is achieved by dynamically altering the resonance frequency, resulting in the on and off modulation of lightwaves [16]. Conversely, when the lifetime of cavity photons exceeds

 © 2024 American Physical Society

the modulation period, resonance frequency shifts during lightwave circulation, intertwining filtering and modulation and complicating its description. Current analytical methods, such as the Heisenberg-Langevin equation [10], temporal coupled-mode theory [17], and the transfer matrix method [18], involve complicated differential equations or matrix manipulation to attain modulation outcomes.

In this Letter, we propose a "virtual state" model, derived from a transfer matrix approach, to simplify dynamic ring modulation descriptions. Virtual state, a fundamental concept in quantum mechanics, describes transition states and plays an essential role in various physical research fields, including material structure, optical phenomena, and quantum computing. Its application has profoundly impacted our understanding of numerous physical phenomena, particularly resonance transitions observed in stimulated Raman scattering [19–22] and two-photon transitions [23,24]. Our proposed model separates modulation from linear time-invariant filtering, eliminating the need for the complex processes necessitated by existing models. Utilizing the virtual state allows visualization of phase modulation experienced by incident light, making the modulation and filtering processes more intuitive. Additionally, our generic model can accurately describe any input signals and modulation formats. We further demonstrate that the ring can be approximated as a phase modulator in cases where the optical input is resonant and the driving signal is not resonant. Resonant modulation experiments and numerical simulations are conducted to assess the precision of our virtual state model.

Principle.—According to our theory, the process of a lightwave passing through a dynamic ring modulator can be expressed as the input lightwave being excited to a virtual state by a cumulative phase and then jumping back to the real state after passing through the corresponding static ring. Mathematically, this model is expressed as follows:

$$E_{\mathrm{out}}(t) = \left[E_{\mathrm{in}}(t)e^{-i\theta(t)}\right] \otimes h_{\mathrm{static}}(t)e^{i\theta(t)}, \tag{1}$$

with

$$\theta(t+\tau) - \theta(t) = \varphi(t). \tag{2}$$

In Eq. (1), $E_{\mathrm{in}}(t)$ and $E_{\mathrm{out}}(t)$ are the input and drop-port output light fields of the dynamic ring modulator, as shown in Fig. 1(a). The actual phase shift $\varphi(t)$ is induced by voltage $V(t)$ and alters the resonance frequency. τ is the round-trip time delay of the static ring. $\theta(t)$ is the assumed phase modulation, which is the accumulation of the actual phase shift. $h_{\mathrm{static}}(t)$ is the zero-modulation impulse response of the ring. $\otimes$ is the convolution operation.

To validate our theory, we assume zero dispersion within the waveguide, with the phase shift located on the ring's right side, as depicted in Fig. 1(a). Despite potential variations in electrode size or position, we propose that the phase shift functions as a whole. The coupling coefficient between the bus waveguide and the ring is called κ, while the loss is called α (where $\alpha = 1$ means zero loss). Utilizing the transfer matrix method [18], we establish a correlation between the input and output light fields:

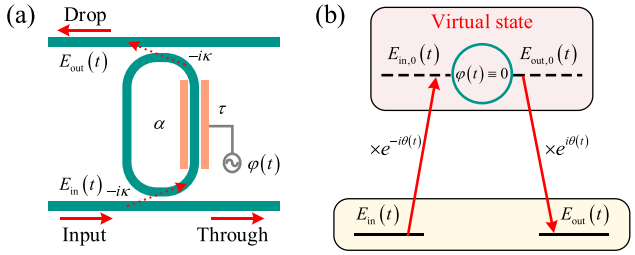

FIG. 1. (a) Structural diagram of the dynamic ring modulator. (b) Diagram of the virtual-state model corresponding to Eq. (1).

$$E_{\mathrm{out}}(t) = \left[\alpha\left(1-\kappa^2\right)E_{\mathrm{out}}(t-\tau) - \alpha^{1/2}\kappa^2 E_{\mathrm{in}}(t-\tau)\right]e^{i\varphi(t-\tau)}. \tag{3}$$

In Eq. (3), the time-varying $\varphi(t)$ prevents further simplification. However, if we uphold Eq. (2) and the definitions

$$E_{\mathrm{in}}(t) = E_{\mathrm{in},0}(t)e^{i\theta(t)}, \tag{4a}$$

$$E_{\mathrm{out}}(t) = E_{\mathrm{out},0}(t)e^{i\theta(t)}, \tag{4b}$$

then we can restate Eq. (3) to describe a static ring where $E_{\mathrm{in},0}(t)$ and $E_{\mathrm{out},0}(t)$ function as the input and drop-port output light fields, respectively, which serve as the virtual states in our model. By combining Eqs. (4), the proposed virtual state model, described by Eq. (1), can be obtained. Our model separates the dynamic ring modulation into two phase modulations and a static filter. The input lightwave is first excited to the virtual state by the cumulative phase, passes through the static ring, and finally jumps back to the real state. This process is illustrated in Fig. 1(b). A similar derivation applies to the through port, as indicated in $E_{\mathrm{out,through}}(t) = \left[E_{\mathrm{in}}(t)e^{-i\theta(t)}\right] \otimes h_{\mathrm{static,through}}(t)e^{i\theta(t)}$.

Distinct from existing analytical methods, the proposed model separates the modulation and linear time-invariant filtering. The cumulative phase modulation, $\theta(t)$, while not directly occurring, is deemed plausible through Eq. (2), as it results from the accumulation of the actual phase shift $\varphi(t)$ in the ring. Since the circulating lightwave is modulated by $\varphi(t)$ with period τ, the cumulative phase modulation $\theta(t)$ correspondingly increases and accounts for Eq. (2). Specifically, if the modulation rate is slower than $1/\tau$, one can approximate $\theta(t+\tau) - \theta(t)$ by $\dot{\theta}(t)\cdot\tau$, so that the cumulative phase can be approximated as

$$\theta(t) \approx \frac{1}{\tau}\int \varphi(t)dt, \tag{5}$$

where $\varphi = -2\pi\tau\Delta f_r$, and Δf_r represents the shift of resonance frequency. Assuming the incident lightwave is initially at the resonance frequency f_r, the transmittance is $H_{\text{static}}(f_r)$. Normally, under dc driving, the resonance peak of the ring shifts by Δf_r, and the corresponding transmittance becomes $H_{\text{static}}(f_r + \Delta f_r)$ when the unchanged lightwave passes through. According to our model, the shift in resonant frequency equates to a change in the state of the input lightwave. The lightwave transitions to the virtual state by $\theta(t)$, traverses the static ring with transmittance $H_{\text{static}}(f_r + \Delta f_r)$, then jumps back to its original state. The virtual-state model can illustrate not only the case of dc modulation but also apply to any complex and rapid modulation.

Compared with other models that rely on complex final calculations to obtain output, our model enables easy and rapid output prediction. This capability assists us in drawing meaningful conclusions about ring modulation. For instance, our model suggests that when the input optical detuning is zero and the driving frequency detuning is nonzero, the ring serves as a phase modulator, with the potential for an enlarged modulation depth. Recently, the bulk of high-Q ring-modulation research has been directed toward narrowband resonant modulation, focusing mainly on the generation of broadband OFC through efficient phase modulation techniques. Regrettably, there exists a considerable void in research and application concerning detuning and broadband modulation, which significantly curtails the potential of ring modulation across various fields and applications. Our model is highly versatile and capable of analyzing a wide range of modulation techniques beyond resonant modulation, including detuning modulation and other complex modulation schemes. For resonant modulation, the lightwave passing through the ring undergoes phase modulation at the frequency of the applied voltage, thus generating numerous comb lines, spaced by the resonant frequency. At frequencies far from the incident lightwave frequency, the power of the comb lines becomes increasingly suppressed and decays exponentially, in line with previously published results [13]. Here, we focus on analyzing detuning modulation. We assume that the detuning modulation results in an actual phase shift of $\varphi_{\text{detuning}}(t) = \beta\cos(\Omega t)$, where β is the modulation depth, $\Omega = 2\pi(\text{FSR} + \Delta)$ is the driving angular frequency, Δ is the detuning frequency, and $\text{FSR} = 1/\tau$ is the free spectral range (FSR) of the static ring. According to Eq. (2), the corresponding cumulative phase is $\theta_{\text{detuning}}(t) = G\beta\sin(\Omega(t - \tau/2))$, where $\beta = (\pi V_{\text{p}}/GV_{\pi})$, V_{p} is the driving peak voltage, V_{π} is the half-wave voltage, G is the phase modulation gain, expressed by

$$G = \frac{1}{2\sin(\Omega\tau/2)}. \tag{6}$$

This equation indicates that when Δ is smaller than FSR/6, the cumulative phase modulation can be increased significantly compared with the actual phase shift. The gain increases as the driving detuning becomes smaller within the range of FSR/2. According to Eq. (1), the lightwave is first phase-modulated by $\theta_{\text{detuning}}(t)$; one then gets an OFC with a frequency interval of Ω. If the optical detuning is zero and the driving detuning is much greater than the ring bandwidth, only the comb line at the incident wavelength can pass through the static ring, while all other comb lines, which are not aligned with any transmission peak, will be suppressed. An approximate solution for the detuning modulation, based on Eq. (1), can be obtained as

$$E_{\text{out}}(t) \propto J_0(G\beta)|H_{\text{static,max}}|e^{iG\beta\sin(\Omega(t-\tau/2))}, \tag{7}$$

where $J_0(G\beta)$ is the zeroth term of the Fourier expansion of $e^{-iG\beta\sin(\Omega(t-\tau/2))}$, corresponding to the amplitude of the comb line that aligns with the incident frequency. $|H_{\text{static,max}}|$ is the maximum value of the frequency response of the static ring. Accordingly, it suggests that the ring modulator can serve as a phase modulator under detuning driving, which is quite distinct from the conventional use of rings as intensity modulators [25]. Moreover, Eq. (7) reveals that the driving signal can generate a quadratic phase term under local approximation, indicating that the resulting phase modulation is equivalent to a time lens [26].

Experiment.—We fabricated a ring modulator on a substrate of a 500-nm-thick X-cut single-crystalline lithium niobate thin film, overlaid on a 4.7-μm-thick buried silicon dioxide layer. In this configuration, the polarization of light within the ring operates in a quasitransverse electric optical mode. The ring features a waveguide loss of roughly 0.8 dB/cm, with a waveguide cross section in the ring area of about 2.4 μm × 0.26 μm and in the input and output regions of around 1.32 μm × 0.26 μm. Figure 2(a) presents an optical micrograph of the device. The circumference of the ring is approximately 13.24 mm, with an electrode length of approximately 6 mm located on one of the racetrack arms.

When we apply varying dc voltages to the ring, we observe an EO efficiency of approximately 430 MHz/V, as shown in Fig. 2(c). The resonant 3-dB linewidth of the ring is 563 MHz, corresponding to a loaded Q factor of 3.4×10^5, and the FSR is 10 GHz. We demonstrate resonant driving based on the experimental setup shown in Fig. 2(b). A tunable laser (CoBrite-DX) is initially resonantly incident, coupled to the chip by a grating. The output is measured by an optical spectrum analyzer (OSA, AP2060A) after an erbium-doped fiber amplifier (EDFA). A sinusoidal wave, generated by a microwave source (SignalCore SC5511A), is transmitted to the electrode of the ring through a microwave probe. We set the input optical power at 13 dBm, with the microwave drive frequency equivalent to the FSR and peak voltages of 4 V and 8 V. The generated comb spectra are shown in Figs. 2(d) and 2(e). To verify the accuracy of our model, we perform two numerical simulations for resonant

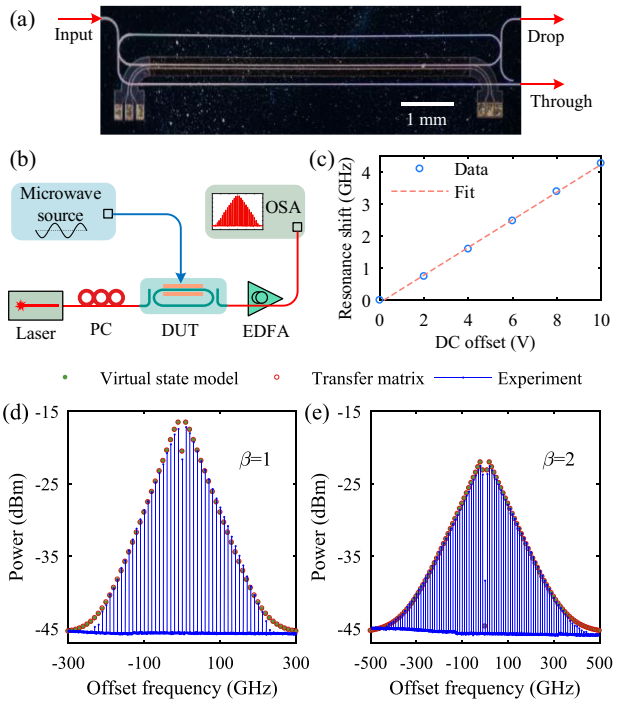

FIG. 2. (a) Optical micrograph of the ring modulator. (b) Experimental setup for high-speed modulation. DUT is the device under test. PC is the polarization controller. (c) Resonant wavelength shift as a function of dc voltage. (d),(e) The output spectrum of the resonant modulation with a resolution of 140 MHz.

modulation. The first, based on our virtual-state model, computes the output spectrum using Eq. (1). The second simulation employs the analytical solution $E_{\mathrm{out}}(t) = \{-\alpha^{1/2}\kappa^2 e^{i\varphi(t)}/[1-\alpha(1-\kappa^2)e^{i\varphi(t)}]\}E_{\mathrm{in}}(t)$ derived from Eq. (3), serving as a comparative reference for our virtual-state model. The corresponding modulation depths for numerical simulations are $\beta = 1$ and $\beta = 2$, respectively. We use parameters for our simulations that align with our experimental measurements: loss coefficient $\alpha = 0.89$, coupling coefficient $\kappa = 0.21$, and FSR = 10 GHz. These parameters correspond to the measured Q factor (3.4×10^5) in our experiment. Notably, our virtual-state model aligns well with both the transfer matrix method and our experimental data, revealing a symmetrical comb that decays approximately exponentially. The subsequent experiments (detuning modulation, phase modulation gain measurements) and their numerical simulations share these resonator parameters.

Subsequently, we measure the detuning drive of the ring modulator and evaluate the potential applications of the approximate solution. Specifically, we employ a driving frequency of 11 GHz ($\Delta = 1$ GHz) and apply peak voltages of 4 V and 8 V. When the laser detuning is set at zero, the output spectra shown in Figs. 3(a) and 3(b) are obtained. We conduct numerical simulations based on the analytical and approximate solutions of detuning modulation, where the modulation depths corresponding

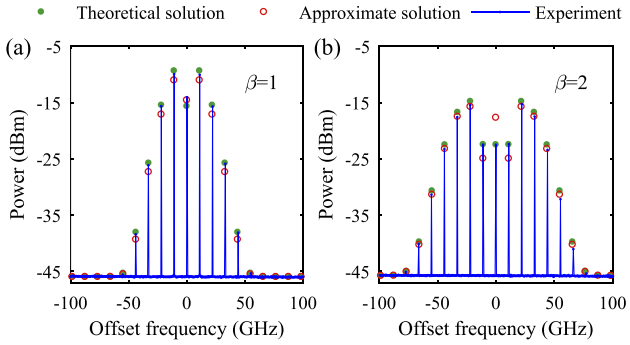

FIG. 3. (a),(b) The output spectrum of the detuning modulation with a resolution of 140 MHz.

to different peak voltages are 1 and 2, respectively. It is shown that the approximate solution is consistent with both theoretical solution and experimental results. In our experiment, the comb span of the detuning modulation is smaller than that of the resonant modulation under the same driving depth. However, the detuning modulation has specific advantages over the resonant modulation, such as the generated OFC having a more concentrated energy distribution in the wavelength domain.

To exemplify the energy-concentrated OFC produced by detuning modulation, we conducted numerical simulations using a high Q ring. The parameters for this high Q ring are $\alpha = 0.997$, $\kappa = 0.053$, and FSR = 10 GHz, yielding a corresponding Q value of 1×10^7. We set the modulation depth at 2.7 and the driving frequency at 10.120 GHz ($\Delta = 120$ MHz). Figure 4 presents the envelope curve of the simulated energy-concentrated OFC, which vividly demonstrates our findings compared to resonant modulation at the same modulation depth. The conversion efficiency of the detuning modulation obtained by the ratio of the frequency comb power to the total input optical power in a 2 THz bandwidth is approximately 12 times that of the resonant modulation. This allows for the creation of an energy-concentrated OFC while maintaining the accuracy

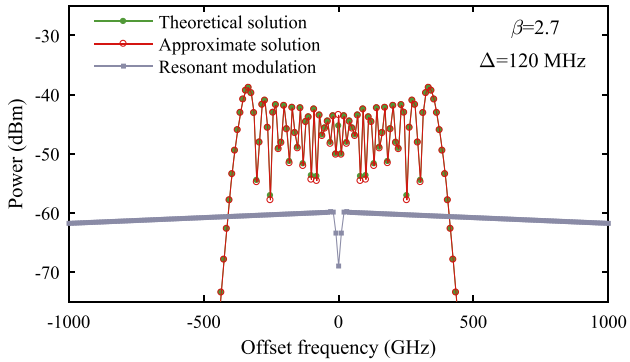

FIG. 4. The output spectrum envelope curves of detuning and resonant modulation of a ring with a Q factor of 1×10^7.

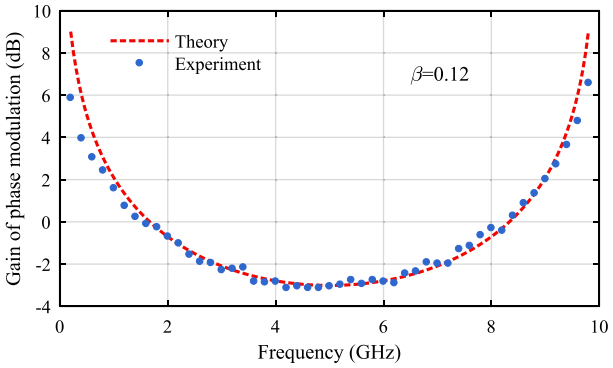

FIG. 5. Experimental and theoretical phase modulation gain curves.

of the approximation even at high modulation depths. In optical communication systems that require high signal transmission distance and speed, energy-concentrated OFCs can effectively mitigate noise and enhance the signal-to-noise ratio, thereby improving system performance and reliability [27]. Moreover, since phase modulation equates to a time lens, an intensity modulator can be cascaded with the system to further flatten the OFC [28,29], which can be highly valuable for optical communication [30], optical arbitrary waveform generation [31], and microwave photonics [32].

Finally, under detuning driving, we experimentally measure the cumulative gain of the phase modulation, finding that the gain follows the driving frequency in good agreement with the numerical simulation of Eq. (6). The driving frequency of both experiments and numerical simulations is swept from 0.2 GHz to 9.8 GHz with a step size of 0.2 GHz. The peak voltage in the experiment is 0.5 V, and the corresponding simulation modulation depth is $\beta = 0.12$. Calculation of the phase modulation gain is based on the output spectra measured at different driving frequencies. Our experimental data are consistent with the theoretical curve according to Eq. (6), as shown in Fig. 5. It should be noted that under the assumption of detuning driving and phase modulation, the accumulation gain is independent of the Q factor, differing from the traditional definition. The gain decreases with an increase in driving detuning. If the modulation frequency differs from the resonance frequency, the gain curve becomes relatively flat, which is beneficial to the phase modulation of broadband driving signals, and may potentially expand the applications of ring modulators to microwave photonics and optical communication [33].

Conclusion.—In this Letter, we propose a novel analytical solution for EO ring modulators, utilizing the virtual state model, a unique concept that decouples intertwined modulation and filtering within ring modulation into two independent processes. We discovered that dynamic ring modulation simplifies into a linear time-invariant response, with input and output modulated by a cumulative phase. The virtual-state model offers valuable insights into the core mechanisms of ring modulators, where the modulated state of lightwave due to the cumulative phase constitutes a "virtual state," facilitating prediction and clarification of resonator behavior. Our analysis method is highly versatile and can be applied to resonators based on various modulation principles, such as tunable superconducting cavities [34], tunable electromagnetic cavities [35], magneto-optical modulated microring resonators [36], and thermo-optical modulated silicon microring resonators [37]. This solution enhances our understanding of ring modulators and aids in their optimization and design for diverse applications. Specifically, it can be utilized for quantitative analysis and optimization design of composite ring resonators, such as cascaded coupling resonators [38], ring modulators with feedback waveguides [39], and ring modulators based on Mach-Zehnder interferometer coupling structures [40]. This approach offers a simplified yet comprehensive framework for exploring the physical insights and improving the performance of these resonant devices.

This work was supported in part by National Key Research and Development Program of China (2018YFA0701902) and National Natural Science Foundation of China (61925505, 62071055).

*These authors contributed equally to this work.
†Corresponding author: ytdai@bupt.edu.cn
‡Corresponding author: ml@semi.ac.cn

[1] D. A. B. Miller, Attojoule optoelectronics for low-energy information processing and communications, J. Lightwave Technol. **35**, 346 (2017).
[2] C. Sun, M. T. Wade, Y. Lee *et al.*, Single-chip microprocessor that communicates directly using light, Nature (London) **528**, 534 (2015).
[3] T. Zhou, X. Lin, J. Wu, Y. Chen, H. Xie, Y. Li, J. Fan, H. Wu, L. Fang, and Q. Dai, Large-scale neuromorphic optoelectronic computing with a reconfigurable diffractive processing unit, Nat. Photonics **15**, 367 (2021).
[4] D. Marpaung, J. Yao, and J. Capmany, Integrated microwave photonics, Nat. Photonics **13**, 80 (2019).
[5] B. Behroozpour, P. A. M. Sandborn, M. C. Wu, and B. E. Boser, Lidar system architectures and circuits, IEEE Commun. Mag. **55**, 135 (2017).
[6] R. Qian, K. C. Zhou, J. Zhang, C. Viehland, A. H. Dhalla, and J. A. Izatt, Video-rate high-precision time-frequency multiplexed 3D coherent ranging, Nat. Commun. **13**, 1476 (2022).
[7] R. Luo, H. Jiang, S. Rogers, H. Liang, Y. He, and Q. Lin, On-chip second harmonic generation and broadband parametric down-conversion in a lithium niobate microresonator, Opt. Express **25**, 24531 (2017).
[8] X. Ye, S. Liu, Y. Chen, Y. Zheng, and X. Chen, Sum-frequency generation in lithium-niobate-on-insulator microdisk via modal phase matching, Opt. Lett. **45**, 523 (2020).

[9] J. Holzgrafe, N. Sinclair, D. Zhu, A. Shams-Ansari, M. Colangelo, Y. Hu, M. Zhang, K. K. Berggren, and M. Lončar, Cavity electro-optics in thin-film lithium niobate for efficient microwave-to-optical transduction, Optica **7**, 1714 (2020).
[10] T. P. McKenna, J. D. Witmer, R. N. Patel, W. Jiang, R. Van Laer, P. Arrangoiz Arriola, E. Alex Wollack, J. F. Herrmann, and A. H. Safavi-Naeini, Cryogenic microwave-to-optical conversion using a triply-resonant lithium niobate on sapphire transducer, Optica **7**, 1737 (2020).
[11] W. C. Jiang and Q. Lin, Chip-scale cavity optomechanics in lithium niobate, Sci. Rep. **6**, 36920 (2016).
[12] M. Li, J. Ling, Y. He, U. A. Javid, S. Xue, and Q. Lin, Lithium niobate photonic-crystal electro-optic modulator, Nat. Commun. **11**, 4123 (2020).
[13] M. Zhang, B. Buscaino, C. Wang, A. Shams-Ansari, C. Reimer, R. Zhu, J. M. Kahn, and M. Lončar, Broadband electro-optic frequency comb generation in a lithium niobate microring resonator, Nature (London) **568**, 373 (2019).
[14] M. Zhang, C. Wang, Y. Hu, A. Shams-Ansari, T. Ren, S. Fan, and M. Lončar, Electronically programmable photonic molecule, Nat. Photonics **13**, 36 (2019).
[15] Y. Hu, M. Yu, D. Zhu, N. Sinclair, A. Shams-Ansari, LB. Shao, J. Holzgrafe, E. Puma, M. Zhang, and M. Lončar, On-chip electro-optic frequency shifters and beam splitters, Nature (London) **599**, 587 (2021).
[16] Y. Zhang, H. Zhang, J. Zhang, J. Liu, L. Wang, D. Chen, N. Chi, X. Xiao, and S. Yu, 240 Gb/s optical transmission based on an ultrafast silicon microring modulator, Photonics Res. **10**, 1127 (2022).
[17] G. Liang, H. Huang, A. Mohanty, M. C. Shin, X. Ji, M. J. Carter, S. Shrestha, M. Lipson, and N. Yu, Robust, efficient, micrometre-scale phase modulators at visible wavelengths, Nat. Photonics **15**, 908 (2021).
[18] Y. Zhang, Q. Liu, C. Mei, D. Zeng, Q. Huang, and X. Zhang, Proposal and demonstration of a controllable Q factor in directly coupled microring resonators for optical buffering applications, Photonics Res. **9**, 2006 (2021).
[19] A. Vivas-Viaña, A. González-Tudela, and C. S. Muñoz, Unconventional mechanism of virtual-state population through dissipation, Phys. Rev. A **106**, 012217 (2022).
[20] A. Najmaie, E. Ya. Sherman, and J. E. Sipe, Generation of spin currents via Raman scattering, Phys. Rev. Lett. **95**, 056601 (2005).
[21] J. Szlachetko, J.-Cl. Dousse, J. Hoszowska, M. Pajek, R. Barrett, M. Berset, K. Fennane, A. Kubala-Kukus, and M. Szlachetko, High-resolution study of x-ray resonant Raman scattering at the K edge of silicon, Phys. Rev. Lett. **97**, 073001 (2006).
[22] E. Riccardi, M.-A. Méasson, M. Cazayous, A. Sacuto, and Y. Gallais, Gate-dependent electronic Raman scattering in graphene, Phys. Rev. Lett. **116**, 066805 (2016).
[23] E. G. Dalla Torre, J. Otterbach, E. Demler, V. Vuletic, and M. D. Lukin, Dissipative preparation of spin squeezed atomic ensembles in a steady state, Phys. Rev. Lett. **110**, 120402 (2013).
[24] C. Thomsen and S. Reich. Double resonant Raman scattering in graphite, Phys. Rev. Lett. **85**, 5214 (2000).
[25] R. Dube-Demers, S. LaRochelle, and W. Shi, Ultrafast pulse-amplitude modulation with a femtojoule silicon photonic modulator, Optica **3**, 622 (2016).
[26] R. Salem, M. A. Foster, and A. L. Gaeta, Application of space–time duality to ultrahigh-speed optical signal processing, Adv. Opt. Photonics **5**, 274 (2013).
[27] L. Lundberg, M. Mazur, A. Mirani, B. Foo, J. Schröder, V. Torres-Company, M. Karlsson, and P. A. Andrekson, Phase-coherent lightwave communications with frequency combs, Nat. Commun. **11**, 201 (2020).
[28] V. Torres-Company, J. Lancis, and P. Andres, Lossless equalization of frequency combs, Opt. Lett. **33**, 1822 (2008).
[29] M. T. Kauffman, W. C. Banyai, A. A. Godil, and D. M. Bloom, Time-to-frequency converter for measuring picosecond optical pulses, Appl. Phys. Lett. **64**, 270 (1994).
[30] T. Ohara, H. Takara, T. Yamamoto, H. Masuda, T. Morioka, M. Abe, and H. Takahashi, Over-1000-channel ultradense WDM transmission with supercontinuum multicarrier source, J. Lightwave Technol. **24**, 2311 (2006).
[31] C.-B. Huang, Z. Jiang, D. Leaird, J. Caraquitena, and A. Weiner, Spectral line-by-line shaping for optical and microwave arbitrary waveform generations, Laser Photonics Rev. **2**, 227 (2008).
[32] V. R. Supradeepa, C. M. Long, R. Wu, F. Ferdous, E. Hamidi, D. E. Leaird, and A. M. Weiner, Comb-based radiofrequency photonic filters with rapid tunability and high selectivity, Nat. Photonics **6**, 186 (2012).
[33] W. D. Sacher and J. K. S. Poon, Microring quadrature modulators, Opt. Lett. **34**, 3878 (2009).
[34] S. Kim, D. Shrekenhamer, K. McElroy, A. Strikwerda, and J. Alldredge, Tunable superconducting cavity using superconducting quantum interference device metamaterials, Sci. Rep. **9**, 4630 (2019).
[35] X. Liu, L. P. Katehi, W. J. Chappell, and D. Peroulis, High-Q tunable microwave cavity resonators and filters using SOI-based RF MEMS tuners, J. Microelectromech. Syst. **19**, 774 (2010).
[36] J. V. S. Neto, W. O. Carvalho, and J. R. Mejía-Salazar, Magnetically tunable micro-ring resonators for massive magneto-optical modulation in dense wavelength division multiplexing systems, Sensors **22**, 8163 (2022).
[37] J. Sun, R. Kumar, M. Sakib, J. B. Driscoll, H. Jayatilleka, and H. Rong, A 128 Gb/s PAM4 silicon microring modulator with integrated thermo-optic resonance tuning, J. Lightwave Technol. **37**, 110 (2018).
[38] Y. Hu, M. Yu, B. Buscaino, N. Sinclair, D. Zhu, R. Cheng, A. Shams-Ansari, L. Shao, M. Zhang, J. Kahn *et al.*, High-efficiency and broadband on-chip electro-optic frequency comb generators, Nat. Photonics **16**, 679 (2022).
[39] H. Hwang, H. Heo, K. Ko, M. R. Nurrahman, K. Moon, J. J. Ju, S. W. Han, H. Jung, H. Lee, and M. K. Seo, Electro-optic control of the external coupling strength of a high-quality-factor lithium niobate micro-resonator, Opt. Lett. **47**, 6149 (2022).
[40] Y. Li, L. S. Stewart, and P. D. Dapkus, High speed silicon microring modulator employing dynamic intracavity energy balance, Opt. Express **20**, 7404 (2012).